Article:
Di Antonio, M, Ponjavic, A orcid.org/0000-0002-7561-1127, Radzevičius, A et al. (8 more authors) (2020) Single-molecule visualization of DNA G-quadruplex formation in live cells. Nature Chemistry, 12 (9). pp. 832-837. ISSN 1755-4330

https://doi.org/10.1038/s41557-020-0506-4

Single-molecule visualisation of DNA G-quadruplex formation in live cells.

Marco Di Antonio[1,4†], Aleks Ponjavic[1,5,6†], Antanas Radzevičius[1†], Rohan T. Ranasinghe[1], Marco Catalano[1], Xiaoyun Zhang[1], Jiazhen Shen[2], Lisa-Maria Needham,[1] Steven F. Lee[1], David Klenerman[1]*, Shankar Balasubramanian[1,2,3]*

1. Department of Chemistry, University of Cambridge, Cambridge CB2 1EW, UK.
2. Cancer Research UK, Cambridge Research Institute, Li Ka Shing Centre, Cambridge CB2 0RE, UK.
3. School of Clinical Medicine, University of Cambridge, Cambridge CB2 0SP, UK.
4. Current affiliation: Imperial College London, Chemistry Department, Molecular Science Research Hub, Wood Lane W12 0BZ, London, UK.
5. Current affiliation: School of Physics and Astronomy, University of Leeds LS2 9JT, Leeds, UK.
6. Current affiliation: School of Food Science and Nutrition, University of Leeds LS2 9JT, Leeds, UK.

† These authors contributed equally to this work.

Abstract

G-rich sequences can form alternative DNA secondary structures called G-quadruplexes (G4s). Substantial evidence now exists to support that formation of G4 structures is related to gene-expression and the case for targeting G4s for therapeutic intervention is getting stronger. Nevertheless, there is a need to devise additional approaches to study G4s in living cells to build further understanding on their actual biological relevance. The *in-situ* observation of G4-formation in living cells would provide evidence that goes beyond observations by immunostaining and ChIP-Seq. Herein, we describe a new G4-specific fluorescent probe (SiR-PyPDS) that has properties that enable single-molecule detection of G4s. We use SiR-PyPDS to achieve real-time detection of individual G4 structures in living cells. Live-cell single-molecule fluorescence imaging of G4s is carried out under conditions that use low concentrations of the G4-binding fluorescent probe (20 nM) that enabled us to provide informative measurements representative of the population of G4s in living cells, without globally perturbing G4 formation and dynamics. Single-molecule fluorescence imaging and time-dependent chemical trapping of unfolded G4s in living cells by means of DMS treatment, revealed that G4s fluctuate between folded and unfolded states. We also demonstrated that G4-formation in live cells is cell-cycle dependent and inhibited by chemical inhibition of transcription and replication. The observation of single fluorescent probes binding to individual G4s provides a new experimental perspective on G4-formation and dynamics in living cells. Our imaging approach will help elucidate the putative roles of individual G4s in real-time in the context of living cells.

Introduction

G-quadruplexes (G4s) are non-canonical structures that can form within guanine-rich nucleic acid sequences (Fig. 1A)[1,2]. Sequencing of G4s in human genomic DNA (G4-Seq) revealed over 700,000 distinct sites that can form G4s, with notable G4-enrichment within gene promoters and at *loci* commonly amplified in cancers[3]. G4 structures have also been imaged *ex vivo* by immunofluorescence with G4-selective antibodies, both in fixed ciliates[4] and, more recently, in fixed human cells[5]. The G4-selective antibody BG4 has been used in chromatin immuno-precipitation followed by sequencing (ChIP-Seq), showing that just ~1% of the G4s identified in purified DNA by G4-Seq could be detected within chromatin[6]. ChIP-Seq experiments rely on measurements integrated over millions of cells and therefore provide only an average view of G4-incidence at a given genomic *loci*. However, G4 homeostasis in cells is likely to be regulated by proteins, such as helicases, so *ex vivo* techniques that provide a snapshot of G4 distribution may hide important dynamic processes that can only be observed by live-cell imaging. Fluorogenic G4-binding probes for the detection of both RNA[7,8] and DNA[9,10] G4s in living cells have been reported. Generally, such probes are used at relatively high (μM) concentrations which can result in global induction of G4-structures, perturbation of endogenous G4-folding dynamics and cellular stress/toxicity through binding to G4s globally. Furthermore, some observational approaches require environmentally responsive probes which can pose limits on the quantitative study of specific G4-formation as well the challenge of disentangling genuine G4-binding from environmental effects. We have pursued single-molecule fluorescence imaging of G4s in living cells to detect individual G4s in the nucleus of living cells at low nanomolar concentrations of fluorescent probe. The use of a G4-specific probe (SiR-PyPDS) and a control probe (SiR-iPyPDS), with poor affinity to G4s, together with ligand competition experiments, confirmed G4s specificity. Relatively low probe concentrations (nM) helps avoid global induction of G4s inherent in ensemble fluorescence methods. Specifically, only a small fraction (~4%) of G4s are bound by the probe, without perturbing global folding dynamics. Herein we report, for the first time, detection of individual G4s in the nucleus of living human cells by single-molecule fluorescence microscopy.

Results and Discussion

SiR-PyPDS (Fig. 1B) was prepared by tethering the red fluorophore Silicon-Rhodamine (SiR)[11] to an analogue of an established G4-ligand, pyridostatin[12] (PyPDS), using linkers of different lengths (Fig. S1 and S2). Upon binding to G4-folded oligonucleotides all SiR-PyPDS analogues (Fig. S2) displayed a modest fluorescence increase (~10 fold), which is insufficient to confidently discriminate bound vs unbound probes in cells, but enabled evaluation of optimal linker length by fluorescence titrations. Binding titrations revealed the six carbon linker of SiR-PyPDS (Fig. 1B) as being optimal for G4-binding selectivity of the PyPDS-scaffold, with good binding towards MYC and KIT-1 and h-TELO G4s with K_d values of 0.63 (± 0.08) μM, 1.0 (± 0.1) μM and 2.0 (± 0.8) μM respectively, and no detectable binding to double- or single-stranded DNA (Fig. S3). SiR-PyPDS displayed a quantum yield of 0.05 in solution that increases to 0.2 when the molecule is bound to MYC G4 (see methods). We also designed and synthesized a novel PyPDS isomer (SiR-iPyPDS, Fig. 1B) that could act as a poor-G4 binding control in live cells experiments to support unambiguous identification of G4-binding events of SiR-PyPDS. Our control analogue (SiR-iPyPDS) differs from SiR-PyPDS simply for the position of the amino side-chains on the quinoline ring. We reasoned that the steric clash of the side-chains in SiR-iPyPDS could prevent the molecule from adopting the flat conformation required for G-tetrad recognition. Fluorescence titrations confirmed a more than 10-fold lower G4-binding affinity of SiR-iPyPDS compared to SiR-PyPDS (Fig. S4).

Given the promising results from ensemble binding experiments by SiR-PyPDS and the negative control analogue SiR-PyPDS, we decided to evaluate the suitability of these probes for single-molecule detection of G4s *in vitro*. To test this, we investigated the binding of SiR-PyPDS or SiR-iPyPDS to a G4-folded oligonucleotide, MYC, immobilized on a PEG/biotin-coated surface, by single-molecule imaging (Fig. 1C-E). We acquired images with a long exposure time (500 ms) to capture only relatively long-lived interactions. At a much lower ligand concentration than what was used in ensemble experiments (250 pM), we could detect on average 867 long-lived SiR-PyPDS spots (Fig. 1F, Supplementary Movie S1) in each field of view (Fig. 1G), but observed a ten-fold reduction in long-lived binding (66 events, $P = 5\times10^{-6}$) for the weaker G4 binder SiR-iPyPDS (Fig. 1I, Supplementary Movie S1). We confirmed that events represented binding of individual probes to MYC by observing single-step photobleaching (Fig. S5). As the MYC sequence was also labelled with Alexa Fluor 488 we could use both FRET (Fig. S6A) and single-molecule FRET (Fig. S6B-D) to visualize direct binding of our probe to MYC. Note that at 250 pM, the labelled fraction, θ, of G4s is about 0.05%, according to the Hill-Langmuir equation $\theta = [L]/(K_d + [L])$, where $[L]$ is the concentration of ligand and K_d is the dissociation constant

for ligand binding to G4s. To further investigate if the number of SiR-PyPDS binding event correlates with the density of G4 targets immobilized on the surface, we varied the surface coverage by mixing the biotinylated MYC G4 with a biotinylated single-stranded DNA strand that does not form a G4, at different ratios (Fig. S7, see Methods). We observed a linear relationship between the number of SiR-PyPDS binding events detected and the concentration of MYC G4 immobilised on the surface, confirming that the number of binding events is proportional to the number of G4s on the surface (Fig. S7) and that this number can be used as a proxy for G4-density. We have also confirmed that the MYC sequence used is folded into a G4 structure as judged by circular dichroism spectroscopy (Fig. S8). The observed number of binding events can therefore be used to assess the concentration of folded G4s on the surface. We next compared the binding of SiR-PyPDS and SiR-iPyPDS to different G4-folding oligonucleotides, including MYC, h-TELO and c-KIT-1. Again, we observed a >20-fold increase in the number of binding events for SiR-PyPDS when compared to the control probe SiR-iPyPDS (Fig. S9). These observations confirm that SiR-PyPDS can be applied to single-molecule imaging of G4s and that the decreased binding affinity of the control analogue SiR-iPyPDS causes a lower number of binding events observed (Fig. S9).

To further validate that long-lived binding events observed with SiR-PyPDS could be ascribed as G4-specific, we attempted to compete out SiR-PyPDS binding to MYC G4 with an excess of the structurally unrelated G4-binding ligand PhenDC3[13]. Gratifyingly, binding of SiR-PyPDS to MYC was abrogated when an excess (10 μM) of the potent G4-ligand PhenDC3 was included as a competitor (16 events, $P = 2\times10^{-6}$, Fig. 1F, Supplementary Movie S2). Furthermore, we measured the number of binding events displayed by SiR-PyPDS when the G4-folding sequence of MYC was mutated to prevent G4-formation. SiR-PyPDS binding was negligible (23 events, $P = 2\times10^{-6}$) for the immobilized single-stranded DNA control (MYC-mut, Fig. 1F, Supplementary Movie S1), which is in agreement with what was observed for SiR-PyPDS ensemble fluorescence titrations (Fig. S3). Both the biotin-MYC and MYC-mut used in this experiment were also functionalized with an Alexa-488 fluorophore. We used the 488 emission to measure the total fluorescence on each coverslip functionalised with either MYC or MYC-mut to ensure comparable density of oligonucleotides on the surface between the different experiments (σ = 10% variation between coverslips, Fig. S7B). Therefore, differences observed in binding events were minimally affected by variations in G4 surface coverage, confirming the suitability of SiR-PyPDS and SiR-iPyPDS control as probes for the single-molecule detection of G4s.

We next sought to determine whether the conditions of relatively low probe concentrations used for single-molecule imaging caused global induction of G4-folding or perturbation of G4-folding dynamics. To investigate this, we used G4-folding oligonucleotides (MYC, h-TELO and c-KIT1) labelled with a Cy5 fluorophore at their 5' end and having an overhang hybridised with a complementary oligonucleotide sequence containing a Cy3 fluorophore at its 3' end. The oligonucleotides form a Cy3-Cy5 FRET system capable of assessing the fraction of folded G4s by measuring FRET efficiency between the two fluorophores[14]. When titrated with increasing concentrations of PyPDS, no significant FRET perturbation was observed for PyPDS concentrations below 3 μM (Fig. S10). Therefore, there is no detectable global induction of G4s when imaging under single molecule conditions (Fig 1J). We studied G4-unfolding dynamics using a FRET system with FAM/TAMRA labelled oligonucleotides that were annealed in 150 mM K^+ to form a stable G4 structure (see Methods). We next added a 10 folds molar excess of DNA sequence complementary to the G4-folding sequence to irreversibly trap the unfolded G4 sequence as dsDNA. This allowed us to measure the unfolding kinetics by monitoring a concomitant decrease in the FRET fluorescence signal, as previously described[14]. We found that μM concentrations of SiR-PyPDS are required to slow down the unfolding rate for the tested G4s structures and that low nM concentrations used for single-molecule experiments do not globally affect the unfolding rate of the tested G4-structures (Table S1). Our data demonstrate that single-molecule imaging can be used to address the pervasive problem of current G4-detection strategies that use relatively high concentrations of affinity probes that might globally perturb G4 folding and dynamics.

We next applied the fluorescent G4-ligands to single-molecule imaging of G4s in live cells (Fig. 2A). First, we investigated the toxicity of SiR-PyPDS and SiR-iPyPDS in U2OS cells over a 24 h treatment at different probe concentrations. Both SiR-PyPDS and SiR-iPyPDS did not elicit any cell death response at nM concentrations, as toxicity could only be observed at concentrations higher than 10 μM (Fig. S11). Based on this, U2OS cells were treated for 30 min with 20 nM of SiR-PyPDS, which resulted in under-labeling of G4s at a density where individual fluorophores were spatially well separated (Fig. 2B). This allowed us to visualize individual probes (SiR-PyPDS or SiR-iPyPDS) binding to targets in the nucleus (Fig. 2B-C, Supplementary Movie S3) using single-molecule imaging (400 frames taken with 100 ms exposure using highly inclined laminated optical sheet (HILO) microscopy)[15]. Single step photobleaching provided evidence of binding events by individual probe molecules in the nucleus (Fig. S12), in spite of the extra-nuclear lysosomal accumulation of SiR-PyPDS (Fig. S13). We first measured the number of

binding events whereby a SiR-PyPDS molecule remained stationary within a 300 nm radius for three or more consecutive frames (i.e. 300 ms), detecting an average of 79 binding events per nuclei (Fig. 2D). Similarly to what was observed *in vitro*, treatment of U2OS cells with SiR-iPyPDS (20 nM) revealed an average of only 2 long-lived binding events in the nucleus (Fig. 2D). To confirm that differences in the number of nuclear binding events between SiR-PyPDS and SiR-iPyPDS were not due to different cellular uptake of the two ligands, we used confocal microscopy and demonstrated that upon 10 μM ligands treatment the total nuclear fluorescence intensity measured was comparable between the SiR-PyPDS and SiR-iPyPDS treatments (Fig. S14). These results are consistent with the *in vitro* observations (Fig. 1F) and corroborate the hypothesis that long-lived SiR-PyPDS binding events could be ascribed to specific G4-binding in cells. To further support this hypothesis, we demonstrated that SiR-PyPDS binding could be abrogated in the presence of 10 μM of the unlabeled competitor G4-ligands PDS[12] or PhenDC3[13] (Fig. S15, Supplementary Movie S4), which is also consistent with what was observed *in vitro*.

We next sought to estimate the fraction of G4-labelled by SiR-PyPDS in living cells as we have done for the *in vitro* studies. To do so, we have assumed that the K_d of SiR-PyPDS remains unchanged in the cellular environment and that the nuclear concentration of the probe is 20 nM. Based on these assumptions and using the relationship $[L]/(K_d + [L])$, the fraction of labelled G4s on a single U2OS cells is around 4%. Using this value for labelled G4 fraction, we have roughly estimated the total number of G4s present in a single cell. As we detect about 10 binding events on average in an image frame within a single focal plane (~ 1μm), there would be around 100 binding events in an entire U2OS cell of diameter ~ 10 μm. Therefore, considering we are labelling around 4% of the total number of targets, we can estimate a total number of G4s in a single cell of ~3000, which is in line with what has been detected in human chromatin (between 1,000 and 10,000 G4s) by G4-ChIP-Seq experiments.[6]

We then compared the temporal dynamics of the interaction between SiR-PyPDS and G4s *in vitro* and in cells, to investigate if characteristic dwell times of SiR-PyPDS binding to G4s *in vitro* could also be detected in cells. Time-lapse imaging was used to observe long-lived events (Fig. 3A, Supplementary Movie S5). *In vitro*, an exposure time of 100 ms and interval of 2 s was used to avoid photobleaching effects (time constant τ_b = 923 s), whereas for cellular experiments a slightly longer interval (3 s, τ_b = 104 s) and also a longer exposure time (500 ms) were needed to limit contributions from unbound ligands[16]. The histogram of SiR-PyPDS dwell times could be well fitted ($R^2 > 0.99$) to a single exponential distribution, yielding a photobleaching-corrected binding lifetime of 6.6±0.5 s in cells (Fig. 3B), which is significantly shorter (~2.5 folds, P =

4×10^{-7}, unpaired t-test) than that observed *in vitro* for binding (15.4±0.6 s) to MYC G4. To investigate further this apparent discrepancy, we carried out *in vitro* binding experiments with other G4-forming sequences. These experiments indicated that the dwell times for SiR-PyPDS binding to hTelo and c-KIT1 were respectively 2.5 and 2 times shorter than MYC and were comparable to dwell times observed in living cells. These experiments suggested that the binding dynamics of SiR-PyPDS to synthetic G4-forming oligonucleotides observed *in vitro* can be recapitulated in cells, further supporting that our assay can detect endogenous G4s.

To gain insight into G4-folding dynamics in living cells, we employed the DNA-methylating agent dimethyl-sulfate (DMS) to irreversibly trap the unfolded G4 state (Fig. 3C). The nucleophilic N7 atoms of guanines are exposed and can be methylated by DMS in single- and double-stranded DNA, but are protected in folded G4s by their participation in Hoogsteen hydrogen bonding (Fig 1A). Thus, transiently unfolded G4s can be methylated and irreversibly prevent further G4 re-folding by blocking Hoogsteen hydrogen bonding at N7s (Fig. 3C). First, we demonstrated that DMS could trap the unfolded G4 state *in vitro* by quantifying binding events of SiR-PyPDS with MYC prior to (300 events) and after (40 events, $P = 0.03$) 20 min treatment with 640 mM (8%) DMS (Fig. 3D). We then examined if a similar DMS-dependent G4 depletion could be recapitulated in living cells, while keeping the DMS concentration lower (20 mM, 0.25%) to prevent cell death. We observed a time-dependent decrease of SiR-PyPDS binding events in U2OS cells within minutes after DMS treatment (Fig 3E, Supplementary Movie S6), with a ~20-fold reduction ($P = 0.006$) in binding events after 20 min exposure. These results suggest that G4s naturally undergo structural fluctuations in cells. This, in turn, makes their specific detection by chemical methods, such as DMS-Seq[17], ineffective, as they will inevitably trap the unfolded state (Fig. 3C).

We further probed dynamic formation of G4s in live U2OS cells through different phases of the cell cycle to gain insights into changes in G4-prevalence during active DNA processing states, such as replication (S phase) and transcription (G1 phase). We first confirmed using confocal microscopy that under different conditions tested there were negligible differences in uptake of the fluorescent G4 ligand (Fig. S14). This ensured that the lack of binding events observed under certain cycle phases or after DMS treatment could be confidently ascribed to a change in G4 prevalence. SiR-PyPDS-treated U2OS cells were synchronized to S, G1/S and G0/G1 phases using previously reported procedures[4] and imaged using single-molecule fluorescence microscopy. During S phase, where the cell is undergoing active replication, significant ($P < 10^{-6}$) binding events could be detected (208 events, Fig. 4A, Supplementary Movie S7). The number of

binding events was slightly reduced (103 events, P = 0.01) when cells are preparing to initiate replication (G1/S phase) and transcription is active (Fig. 4B, Supplementary Movie S7). There were negligible ($P < 10^{-6}$) binding events during G0/G1 phase (3 events, Fig. 4C, Supplementary Movie S7), where cellular processes are quiescent. These results show that G4 formation is associated with both transcription and replication and is in agreement with previous observations reported in fixed cells[4,18]. To further confirm the suppression of G4s in the absence of actively processed DNA, we treated unsynchronized U2OS cells with a global replication inhibitor aphidicolin and also the global transcription inhibitor DRB as previously described[17], in order to mimic the quiescent state that characterizes cells undergoing G0 phase. Upon transcription and replication arrest few binding events were detected (3 events, $P < 10^{-6}$), further demonstrating that actively processed DNA is pivotal for G4 formation in living cells (Fig. 4C-D, Supplementary Movie S7).

Conclusions

We have used fluorescent probe molecules to visualise individual G4 structures in living cells, for the first time, using single-molecule fluorescence imaging. The sensitivity of single-molecule methods enabled us to image single binding events to G4 structures at probe concentrations orders of magnitude lower than normally used in biophysical and cellular experiments, thereby minimizing global perturbation of G4s. We applied our new imaging platform to demonstrate that G4-formation is cell-cycle dependent and that the presence of G4s is directly related to fundamental biological processes such as active transcription and replication, as chemical inhibition of these processes led to abrogation of detectable G4s in living cells. Trapping of unfolded G4s by means of DMS methylation revealed that G4s undergo dynamic fluctuations in live cells and that essentially all G4s are trapped in the unfolded state during the course of 20 min DMS treatment (0.25%, 20 mM). We anticipate that further application of this imaging platform will help unravel specific biological functions regulated by individual G4s within the human genome in real-time.

Supplementary Information is available in the online version of the paper.

Acknowledgements Supported by programme grant funding from Cancer Research UK (C9681/A18618, S.B.) core funding from Cancer Research UK (C14303/A17197, S.B.), a Royal Society University Research Fellowship (UF120277 to S.F.L.), Research Professorship (RP150066 to D.K.), a EPSRC (EP/L027631/1 to D.K.) and a BBSRC David Phillips Fellowship (BB/R011605/1 to M.D.A)

Author Contributions M.D.A. performed the design, synthesis and biophysical characterization of G4 ligands. A.P. developed the optical setups used for imaging. M.D.A., A.P. and R.T.R. performed *in vitro* imaging experiments. R.T.R. carried out surface preparation for in vitro experiments. M.D.A. and A.P. performed imaging experiments in cells. A.P. analyzed imaging data. M.C. A.R. and X.Z. contributed to the synthesis and biophysical validation of the ligands. M.D.A., A.P., R.T.R., S.F.L., D.K. and S.B. contributed to the study design. J.S. assisted with DMS experiments. A.R. contributed to cellular staining and imaging. A.R and L.N characterized the fluorescence properties of the G4 ligands. M.D.A., A.P., D.K. and S.B. interpreted the results and co-wrote the manuscript with input from all authors.

Author information: The data reported in this paper is available in the main text or in the supporting information. Reprints and permissions information is available at www.nature.com/reprints. S.B. is a founder and shareholder of Cambridge Epigenetix Ltd. Correspondence and requests for materials should be addressed to S.B. (sb10031@cam.ac.uk) and D.K. (dk10012@cam.ac.uk).

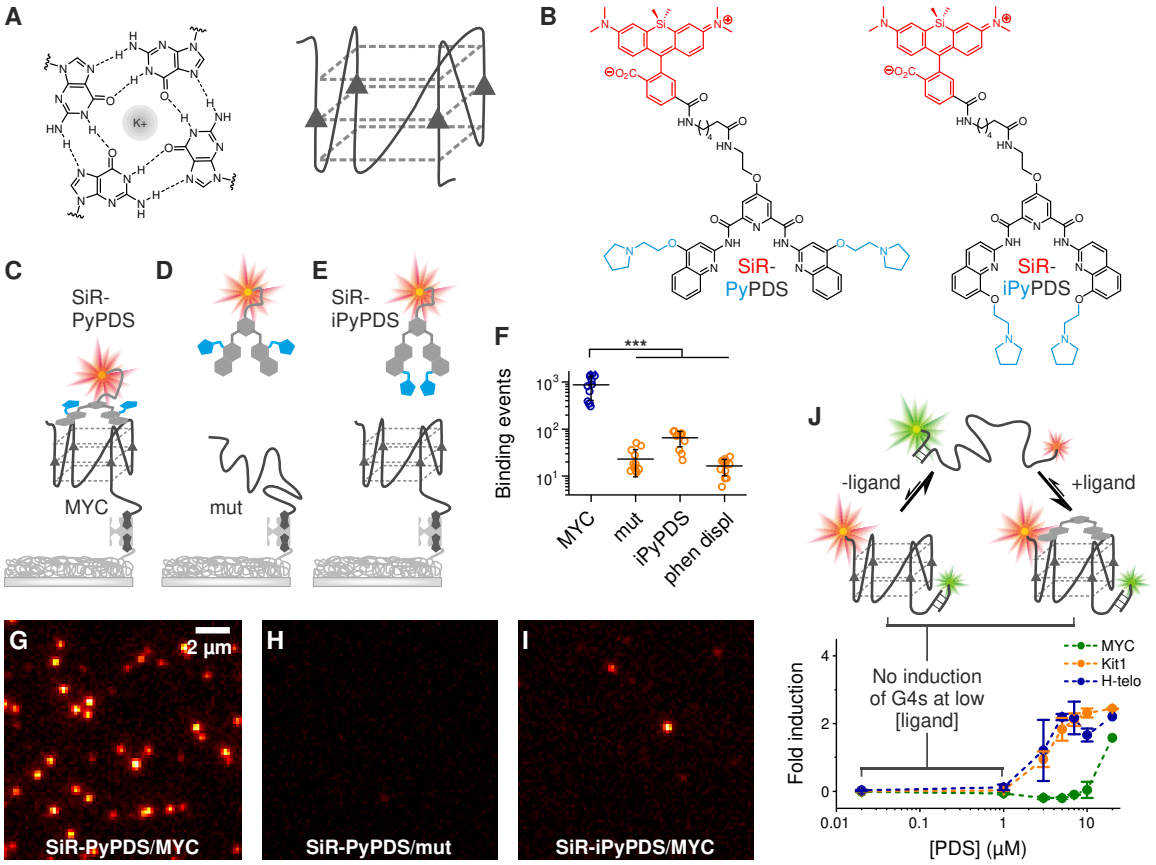

Figure 1. *In vitro* single-molecule fluorescence imaging of G-quadruplexes. (A) Schematic representation of a G-tetrad (left) and a G4 structure (right). (B) Chemical structure of the selective G4-fluorogenic ligand SiR-PyPDS (left) and its inactive isomer, SiR-iPyPDS (right). (C) Schematic of methodology used for visualizing individual G4s. Pre-folded G4 MYC is attached to a coverslip via a biotin-neutravidin linker. The fluorescent G4-probe SiR-PyPDS binds to G4 MYC, which can be visualized using single-molecule fluorescence imaging. (D) SiR-PyPDS will not bind single stranded mutated-MYC that cannot form a G4. (E) The inactive isomer SiR-iPyPDS with its 10 times reduced binding affinity is less likely to bind G4 MYC. (F) Quantification of SiR-PyPDS binding to the G4 MYC ii) SiR-PyPDS binding to the mutated-MYC; iii) SiR-iPyPDS binding to the G4 MYC; iv) SiR-PyPDS binding to the G4 MYC in the presence of 10 μM unlabeled PhenDC3 competitor. Error bars indicate mean ± sd. *** $P < 10^{-5}$, unpaired t-test. (G) Representative images (500 ms exposure) of individual SiR-PyPDS molecules (250 pM) binding to a surface coated with pre-folded MYC G4 oligonucleotide; individual fluorescent puncta indicate binding of single SiR-PyPDS molecules. (H) SiR-PyPDS (250 pM) binding to mutated-MYC. (I) SiR-iPyPDS (250 pM) binding to pre-folded MYC. (J) Interactions of G4 ligands and G4s can alter the equilibrium between unfolded and folded G4s.

Changes in the FRET ratio can be observed at μM PDS concentrations for Kit1 and hTelo and larger concentrations for MYC, indicative of G4 induction, which does not occur at lower concentrations.

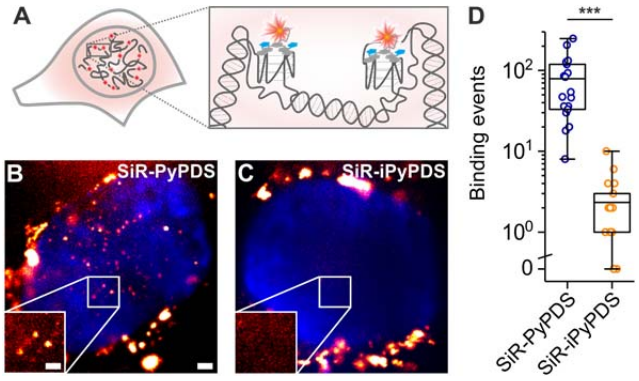

Figure 2. Single-molecule fluorescence imaging of G-quadruplexes in living cells using the fluorescent probe SiR-PyPDS. (A) Schematic of G4s in the cell nucleus with a zoom-in showing G4s stained by SiR-PyPDS. (B) Representative background-subtracted image (max projection of 100 frames with 200 ms exposure) of SiR-PyPDS binding events in a living U2OS cell treated with 20 nM SiR-PyPDS for 30 min before imaging; fluorescent puncta indicate binding of single SiR-PyPDS molecules. Blue color corresponds to nuclear staining with Hoechst 33342. Scale bar is 2 μm. Inset scale bar is 1 μm. C) Representative image of SiR-iPyPDS staining in living U2OS cell treated with 20 nM SiR-PyPDS for 30 min before imaging. (D) Quantification of the binding events within the nucleus lasting more than one frame (100 ms per frame) per cell for SiR-PyPDS and SiR-iPyPDS. Center lines indicate the median; boxes show interquartile range; whiskers denote 5th and 95th percentiles. *** $P < 10^{-5}$, Mann-Whitney U-test.

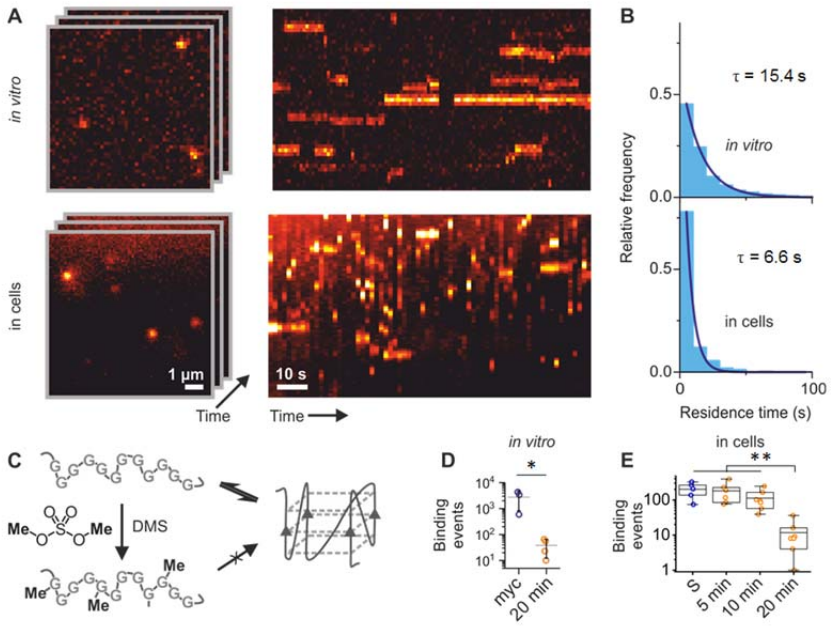

Figure 3. G-quadruplexes in living cells undergo dynamic folding/unfolding. (A) Single-molecule time-lapse imaging of SiR-PyPDS *in vitro* (top) and in cells (bottom). Individual images from the time-lapse stack are shown on the left and kymographs on the right show the dynamic binding kinetics of SiR-PyPDS to G4s. (B) The histograms of dwell times for each experiment (3 positions on a cover slip for *in vitro* and 6 cells for the cell experiment) were fitted with a single-exponential fit to determine the binding lifetime in each condition. (C) Schematic of DMS-meditated chemical trapping of unfolded G4s. (D) Quantification of G4-binding events for untreated and 600 mM DMS-treated G4 MYC for 20 min. Error bars indicate mean ± sd. * $P < 0.05$, Mann-Whitney U-test. (E) Quantification of G4-binding events detected in living cells upon increased exposure to DMS (20 mM), showing a clear time-dependent depletion of G4s. Center lines indicate the median; boxes show interquartile range; whiskers denote 5th and 95th percentiles. ** $P < 0.01$, Mann-Whitney U-test.

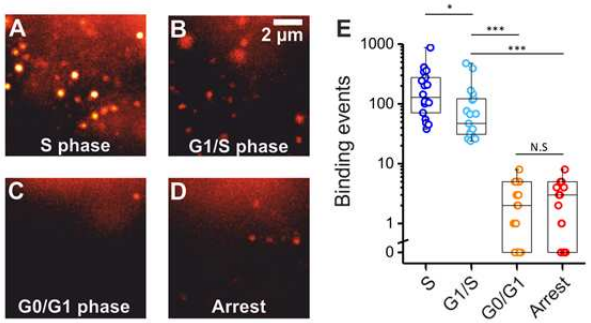

Figure 4. The observation of G4s in live cells is altered by the cell cycle phase and transcription. Representative single-molecule images of G4-binding events are shown for synchronized U2OS cells in (A) the S phase, (B) the G1/S phase, (C) the G0/G1 phase and (D) for unsynchronized cells treated with both the transcriptional inhibitor DRB and the replication inhibitor Aphidicolin. (E) Quantification of binding events lasting more than two frames (100 ms per frame) per cell in living U2OS cells at different cell-cycle phases and after transcription/replication arrest. Center lines indicate the median; boxes show interquartile range; whiskers denote 5th and 95th percentiles. *** $P < 10^{-5}$, * $P < 0.05$, N.S $P > 0.95$ Mann-Whitney U-test.

Methods

Detailed synthetic protocols and purification methodologies for the preparation of SiR-PyPDS and SiR-iPyPDS, biophysical methods and more detailed protocols are described in supporting information.

In vitro single-molecule fluorescence imaging

Binding of G4 ligands to synthetic biotinylated oligonucleotides was imaged at single-molecule resolution by total internal reflection fluorescence microscopy (TIRFM) on glass coverslips coated with polyethylene glycol (PEG) and NeutrAvidin. In this study, we used two different PEG coating procedures (see SI): one based on passive adsorption (Coating method 1, used for data in Fig. 1, 3 and S5) and the other on covalent coupling (Coating method 2, used for data in Fig. S6, S7 and S9). We found similar surface densities of immobilized biotinylated oligonucleotides and degrees of non-specific binding on each surface. Buffers for surface treatment and imaging were freshly filtered each day (0.02 µm syringe filter, Whatman, Cat. No.

6809–2101). Each biotinylated surface was then treated in the same way prior to single-molecule imaging. Wells were first coated with 10 µL of 0.2 mg/mL NeutrAvidin (ThermoFisher, Cat. No. 31000) in 1x PBS containing 0.05% tween-20 for 5 min, washed twice with 10 µL of 1x PBS containing 0.05% tween-20, then treated with 10 µL of 1x PBS containing 1% tween-20 for 10 min. Biotinylated oligonucleotides (c-MYC or c-MYC-mutant, annealed overnight at 100 nM concentration in 100 mM KCl and 50 mM KH_2PO4, pH 7.4) were then diluted to 10 nM in 1x PBS containing 0.05% tween-20 and 10 µL added to each well for 5 min. The wells were then washed twice with 10 µL of 1x PBS containing 0.05% tween-20, then treated with 10 µL of 1x PBS containing 1% tween-20 for 10 min. The wells were then washed once with 250 pM of G4 ligand solutions (SiR-PyPDS or SiR-iPyPDS) in PBS and the solution was finally replaced with 9 µL of G4 ligand at 250 pM in PBS. For *in vitro* ligand displacement experiments, 1 µl of 1mM PhenDC3 was added to the well. For DMS trapping the pre-annealed MYC oligonucleotide (100 nM) was treated with DMS 8% for 20 minutes, quenched by adding 10% β-mercapto-ethanol and used for surface coating.

The general setup used for TIRFM has been described previously[19]. For the *in vitro* experiments TIRFM was implemented on a Nikon Eclipse Ti2 inverted microscope with a Perfect Focus System for maintaining focus during acquisition. 488 nm (MLD 488-200, Cobolt) and 640 nm (LBX-638-180-CSB-PP, Oxxius) lasers were used for excitation with clean-up filters. The emission collected by the 1.49 NA oil immersion 60× (90× with internal magnification) objective lens (Nikon) was filtered with long-pass and band-pass filters (520/36 – 67030 and 692/40 – 67038, Edmund Optics) and imaged on an Evolve 512 Delta EMCCD (Photometrics) with a pixel size of 178 nm, confirmed using a Ronchi ruling. The excitation power density was measured by determining the excitation power after the objective and the beam size in the imaging plane, taking ~4-fold near-field enhancement into account. For binding event measurements, a field of view was acquired for each condition with 500 ms exposure time at a power density of 1.4 kW/cm^2. For longer residency time measurements, time lapses of 300 frames were acquired every 2 s with an exposure time of 100 ms and a power density of 0.4 kW/cm^2. For shorter residency time measurements, time lapses of 300 frames were acquired every 100 ms with an exposure time of 100 ms and a power density of 0.4 kW/cm^2.

Live Cell Imaging

In a typical experiment ~200.000 U2OS cells diluted in 2 ml of DMEM were plated in a 35 mm dish with a 14mm Glass coverslip at the bottom (MatTek) and allowed to adhere overnight. After

~18h, the media was replaced with 2 ml of fresh DMEM media containing SiR-PyPDS or SiR-iPyPDS at a final concentration of 20 nM and cells where further incubated for 30 min. The DMEM media containing SiR molecules was then discarded and cells were washed 2X with PBS pre-warmed at 37 °C. Finally, the media was replaced with PBS containing Hoechst 2μM for nuclear staining, pre-warmed at 37 °C, which was immediately followed by imaging.

The effect of DMS on cellular G4 prevalence was evaluated by treatment prior to SiR-PyPDS labelling: cells were incubated with DMEM containing 20 mM DMS for the indicated time (5, 10 or 20 min). After the desired treatment time DMS was quenched by adding 10% β-mercapto-ethanol in PBS followed by 2X washing with PBS pre-warmed at 37 °C.

Cell cycle synchronisation was performed with mimosine treatment as previously described[4]. Transcriptional and replication arrest was achieved by co-treatment of cells with DRB and Aphidicolin as previously described[17].

Binding of SiR-PyPDS to nuclear G4s was visualised using highly inclined laminated optical sheet (HILO) microscopy[15]. The microscope setup used has been described previously[20]. The central plane of the nucleus in U2OS cells was found with either bright-field microscopy or using Hoechst staining. For binding event measurements, 400 frames were acquired for each cell with 100 ms exposure time at a power density of 180 W/cm^2. For residency time measurements, time lapses of 70 frames were acquired every 3 s with an exposure time of 500 ms and a power density of 180 W/cm^2.

References:

1. Sen, D., Gilbert, W. Formation of parallel four-stranded complexes by guanine-rich motifs in DNA and its implications for meiosis. *Nature* **334**, 364-366 (1988).
2. Hänsel-Hertsch, R., Di Antonio, M., Balasubramanian, S. DNA G-quadruplexes in the human genome: detection, functions and therapeutic potential. *Nat. Rev. Mol. Cell Biol.* **18**, 279-284 (2017).
3. Chambers, V. S., Marsico, G., Boutell, J. M., Di Antonio, M., Smith, G. P., Balasubramanian, S. High-throughput sequencing of DNA G-quadruplex structures in the human genome. *Nat. Biotechnol.* **33**, 877-881 (2015).
4. Schaffitzel, C., Berger, I., Postberg, J., Hanes, J., Lipps, H.J., Plückthun, A. In vitro generated antibodies specific for telomeric guanine-quadruplex DNA react with Stylonychia lemnae macronuclei. *Proc. Natl. Acad. Sci U. S. A.* **98**, 8572-8577 (2001).
5. Biffi, G., Tannahill, D., McCafferty, J., Balasubramanian, S. Quantitative visualization of DNA G-quadruplex structures in human cells. *Nat. Chem.* **3**, 182-186 (2013).

6. Hänsel-Hertsch, R. *et al.* G-quadruplex structures mark human regulatory chromatin. *Nat. Genet.* **48**, 1267-1272 (2016).
7. Chen, X. C. *et al.* Tracking the dynamic folding and unfolding of RNA G-quadruplexes in live cells. *Angew. Chem. Int. Ed.* **57**, 4702–4706 (2018).
8. Laguerre, A. *et al.* Visualization of RNA G-quadruplexes in live cells. *J. Am. Chem. Soc.* **137**, 8521−8525 (2015).
9. Zhang, S. *et al.* Tang, Real-time monitoring of DNA G-quadruplexes in living cells with a small-molecule fluorescent probe. *Nucleic Acids Res.* **46**, 7522-7532 (2018).
10. Shivalingam, A. *et al.* The interactions between a small-molecule and G-quadruplexes are visualized by fluorescence lifetime imaging microscopy. *Nat. Commun.* **6**, 8178 (2015).
11. Lukinavičius, G. *et al.* A near-infrared fluorophore for live-cell super-resolution microscopy of cellular proteins. *Nat. Chem.* **5**, 132-139 (2013).
12. Rodriguez, R., Müller, S., Yeoman, J. A., Trentesaux, C., Riou, J. F., Balasubramanian, S. A novel small molecule that alters shelterin integrity and triggers a DNA-damage response at telomeres. *J. Am. Chem. Soc.* **130**, 15758−15759 (2008).
13. De Cian, A., Delemos, E., Mergny, J. L., Teulade-Fichou, M. P., Monchaud, D. Highly efficient G-quadruplex recognition by bisquinolinium compounds. *J. Am. Chem. Soc.* **129**, 1856−1857 (2007).
14. Ying, L., Green, J. J., Li, H., Klenerman, D., Balasubramanian, S. Studies on the structure and dynamics of the human telomeric G-quadruplex by single-molecule fluorescence resonance energy transfer. *Proc. Natl. Acad. Sci U. S. A.* **100**, 14629-14634 (2003).
15. Tokunaga, M., Imamoto, N., Sakata-Sogawa, K. Highly inclined thin illumination enables clear single-molecule imaging in cells. *Nat. Methods* **5**, 159-161 (2008).
16. Etheridge, T. J. *et al*. Quantification of DNA-associated proteins inside eukaryotic cells using single-molecule localization microscopy. *Nucleic Acids Res.* **42** e146 (2014).
17. Guo, J. U., Bartel, D.P. RNA G-quadruplexes are globally unfolded in eukaryotic cells and depleted in bacteria. *Science* **353**, pii: aaf537 (2016).
18. Rodriguez, R. *et al*. Small-molecule-induced DNA damage identifies alternative DNA structures in human genes. *Nat. Chem. Biol.* **8**, 301-310 (2012).
19. Ponjavic, A. *et al*. Single-Molecule Light-Sheet Imaging of Suspended T Cells. *Biophys. J.* **114**, 2200-2211 (2018).
20. Ponjavic, A., Ye, Y., Laue, E., Lee, S. F., Klenerman, D. Sensitive light-sheet microscopy in multiwell plates using an AFM cantilever. *Biomed. Opt. Express* **9,** 5863-5880 (2018).